Chinese Journal of Mechanical Engineering

ORIGINAL ARTICLE

Open Access

Experimental Study on the Electrochemical Performance of PEMFC under Different Assembly Forces

Tongze Su[1], Jiaran Liu[1], Yanqiang Wei[1], Yihuizi Li[1], Weichao Luo[1] and Jinzhu Tan[1*]

Abstract

Proton exchange membrane fuel cell (PEMFC) is of paramount significance to the development of clean energy. The components of PEMFC are assembled using many pairs of nuts and bolts. The assembly champing bolt torque is critical to the electrochemical performance and mechanical stability of PEMFC. In this paper, a PEMFC with the three-channel serpentine flow field was used and studied. The different assembly clamping bolt torques were applied to the PEMFC in three uniform assembly bolt torque and six non-uniform assembly bolt torque conditions, respectively. And then, the electrochemical performance experiments were performed to study the effect of the assembly bolt torque on the electrochemical performance. The test results show that the assembly bolt torque significantly affected the electrochemical performance of the PEMFC. In uniform assembly bolt torque conditions, the maximal power density increased initially as the assembly bolt torque increased, and then decreased on further increasing the assembly torque. It existed the optimum assembly torque which was found to be 3.0 N·m in this work. In non-uniform assembly clamping bolt torque conditions, the optimum electrochemical performance appeared in the condition where the assembly torque of each bolt was closer to be 3.0 N·m. This could be due to the change of the contact resistance between the gas diffusion layer and bipolar plate and mass transport resistance for the hydrogen and oxygen towards the catalyst layers. This work could optimize the assembly force conditions and provide useful information for the practical PEMFC stack assembly.

Keywords Proton exchange membrane fuel cell, Assembly force, Experiment, Electrochemical performance

1 Introduction

The Sixth Assessment Report of the Intergovernmental Panel on Climate Change (IPCC) [1], published in 2022, warns that global climate change is occurring faster than previously expected. At the same time, several ecological areas are increasingly approaching their critical points, as the global average surface temperature rise will reach or exceed 1.5 ℃ in the next 20 years. The climate crisis will leave millions of people in a situation of acute food and water insecurity. The development of clean energy is at the forefront of countries' medium and long-term plans to achieve carbon neutrality target. Proton exchange membrane fuel cell (PEMFC) is one of the most promising clean energy devices with the advantages about lower operating temperature, high power density and low pollution. PEMFCs are widely used in common household products such as cars, portable electronics, small power stations, etc. Although there have been significant developments in PEMFC technology and commercial rollout has begun, there is still room for improvement in some problems such as life, cost, and performance [2–5]. The US Department of Energy (DoE) life targets for PEMFC are 80000 h for distributed power systems, 30000 h for heavy-duty trucks and no less than 25000 h for public transportation applications under real-world operating

*Correspondence:
Jinzhu Tan
tjznjut@njtech.edu.cn
[1] Nanjing Tech University, Nanjing 211816, China

condition [6]. The assembly and operation environment of the fuel cell may cause the stresses in the PEMFC, which have a great impact on the durability of the PEMFC.

PEMFCs are typically assembled by bolts, which require assembly forces to be applied to each bolt during assembly process. The mechanical stress is caused by bolt assembly forces during the assembly procedure of the PEMFC, which have a significant impact on the electrochemical performance of the PEMFC [2, 4, 7–15]. Zhang et al. [3] developed a thermal-mechanical coupling finite element (FE) model to study the thermal effects of electrochemical reactions. The study found that the contact pressure and stress distributions were similar for single fuel cell and fuel cell stack, and the contact pressure distribution was more uniform for the membrane electrode assembly (MEA) after assembly. The chemical reactions inside the fuel cell were more favourable. Mahmoudi et al. [16] developed a 2D, isothermal, multi-phase and multi-component model to numerically study the effect of non-uniform compression of the gas diffusion layer (GDL) on the cell performance and water management. Their study found that a reasonable flow field structure squeezing the GDL created a more uniform deformation distribution, resulting in a lower contact resistance and less handicap to mass transfer. In order to attain the uniform compression of GDL, appropriate assembly forces are required. Zhang et al. [17] approached to obtain the relationship between the contact resistance and pressure distribution through experimental studies. Chien et al. [18] investigated numerically the correlation between the bolt force and the conductivity and porosity of the GDL and found that the compressing ratio of the GDL linearly increased with the bolt assembly force. The average porosity of GDL decreased linearly with increasing bolt assembly force, while the total contact resistance decreased with increasing bolt assembly force non-linearly. Zhang et al. [19] found that the combined effect of clamping force and flow field resulted in non-uniform mesopore distribution, mass concentration distribution and current density distribution, and led to lateral currents in the proton exchange membrane (PEM) and GDL. Through numerical studies, Zhou et al. [20] found that too large or too small assembly force for different thicknesses of GDL affected the contact resistance and the mass transfer efficiency of the GDL, and that the existence of an optimum assembly force optimized the fuel cell electrochemical performance. Cha et al. [21] verified the effect of assembly force on the contact resistance and mass transfer efficiency of GDL through electrochemical performance experiments and electrochemical impedance spectroscopy (EIS) studies, and also concluded that the relative humidity (RH) had important effect on the choice of clamping force. Zhang et al. [22] established a force-temperature-humidity multi-field coupled model which base on finite element analysis (FEA) and computational fluid dynamics (CFD) for the fuel cell electrochemical performance. Mallick et al. [23] experimentally studied the electro chemical performance of direct methanol fuel cell under non-uniform bolt forces by EIS. Atyabi et al. [24] studied the effect of clamping pressure on the contact resistance between the GDL and the bipolar plate (BPP) by simulation of 3D multi-phase model of the fuel cell. Kulkarni et al. [25] carried out finite element simulations of a multi-phase, non-isothermal electrochemical performance model of MEA under assembly forces through an integrated modelling approached to investigate the effect of assembly forces on MEA. Chen et al. [26] discovered that the nickel metal foam flow field had better water management than the conventional flow field under the assembly force and also had a protective impact on the MEA through a comparative study. Shi et al. [27] studied the effect of assembly pressure and flow field structure on performance of PEMFC. They found that the variation of the width and depth of the channel under the assembly pressure had an impact on the PEMFC electrochemical performance. In the meanwhile, the assembly pressure caused the mesopore of the GDL to be unevenly distributed, which was more good for the water management of the GDL. Zhang et al. [28] established an equivalent stiffness model for contact pressure, which could be predicted simply and quickly compared with the FEA model. Zhang et al. [29] obtained the gas diffusion coefficients in a 3D model by introducing nonlinear stress-strain curves into a 2D simulation based on a combination of FEA and CFD, indicating the effect of assembly force on liquid water and temperature distribution.

Although the effect of assembly force on the fuel cell performance has been reported by lots of articles, most of these researches are based on the ideal situation where the assembly force on each bolt of the fuel cell is identical value. However, on the real conditions, it is difficult to ensure that the assembly force on each bolt is identical. The non-uniform assembly bolt force (torque) may affect the electrochemical performance and mechanical stability of the PEMFC. So it is necessary to investigate the electrochemical performance of PEMFC under different assembly forces. In this paper, a PEMFC with the three-channel serpentine flow field was used and studied. The different assembly clamping bolt torques were applied to the fuel cell in three uniform assembly bolt torque and six non-uniform assembly bolt torque conditions, respectively. And then, the electrochemical performance experiments were performed to study the effect of the assembly bolt torque on the electrochemical performance.

2 Description of Assembly Force Design

A single PEMFC with a three-channel serpentine flow field was used and investigated in this work. The PEMFC consisted of two current collectors, two end plates, two BPPs, a MEA, two elastomeric gaskets and bolts and nuts. The components of the PEMFC were assembled using the eight pairs of bolts and nuts. The eight bolts configuration in the PEMFC was shown in Figure 1. The N1 to N8 in Figure 1 represents the first bolt to the eighth bolt in this work, respectively.

In order to investigate the effect of different assembly bolt torque on the PEMFC electrochemical performance, the various assembly clamping bolt torques were applied to the PEMFC using a digital torque wrench. Figure 2 presents the uniform assembly clamping bolt torque conditions. Figure 2(a) represents the first assembly torque condition in which the assembly torque of each bolt is 2.0 N·m. Similarly, Figure 2(b) represents the second assembly torque condition in which the assembly torque of each bolt is 3.0 N·m. And Figure 2(c) represents the third assembly torque condition in which the assembly torque of each bolt is 4.0 N·m.

Non-uniform assembly bolt torque may lead to uneven assembly pressure between components in PEMFC. In order to analyze the effect of non-uniform assembly force on the performance of fuel cell, six non-uniform assembly bolt torque conditions were considered in this work. Figure 3 presents the non-uniform assembly clamping bolt torque conditions. Figure 3(a) represents the fourth assembly torque condition in which N1 bolt (i.e., the first bolt) and N2 bolt (i.e., the second bolt) were applied to 2.0 N·m, respectively, other bolts (i.e., N3 to N8 bolt) were applied the same torque of 3.0 N·m, respectively. Figure 3(b) represents the fifth assembly torque condition in which N1, N2, N3 and N4 bolt (i.e., the first to fourth bolt) were applied to 2.0 N·m, respectively, other bolts (i.e., N5 to N8 bolt) were applied the same torque of 3.0 N·m, respectively. Figure 3(c) represents the sixth assembly torque condition in which N1, N2, N3, N4, N5 and N6 bolt (i.e., the first to sixth bolt) were applied to 2.0 N·m, respectively, other bolts (i.e., N7 and N8 bolt) were applied the same torque of 3.0 N·m, respectively.

Similarly, Figure 3(d) represents the seventh assembly torque condition in which N1 bolt (the first bolt) and N2 bolt (the second bolt) were applied to 4.0 N·m, respectively, other bolts (i.e., N3 to N8 bolt) were applied the same torque of 3.0 N·m, respectively. Figure 3(e) represents the eighth assembly torque condition in which N1, N2, N3 and N4 bolt (i.e., the first to fourth bolt) were applied to 4.0 N·m, respectively, other bolts (i.e., N5 to N8 bolt) were applied the same torque of 3.0 N·m, respectively. Figure 3(f) represents the ninth assembly torque condition in which N1, N2, N3, N4, N5 and N6 bolt (i.e., the first to sixth bolt) were applied to 4.0 N·m, respectively, other bolts (i.e., N7 and N8 bolt) were applied the same torque of 3.0 N·m, respectively.

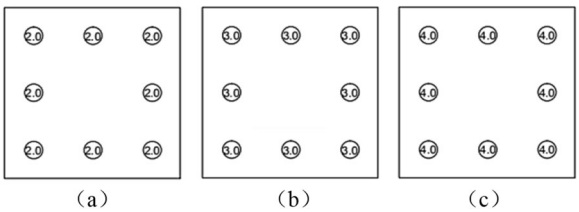

Figure 2 Uniform assembly bolt torque conditions: (**a**) The first condition, (**b**) The second condition, (**c**) The third condition

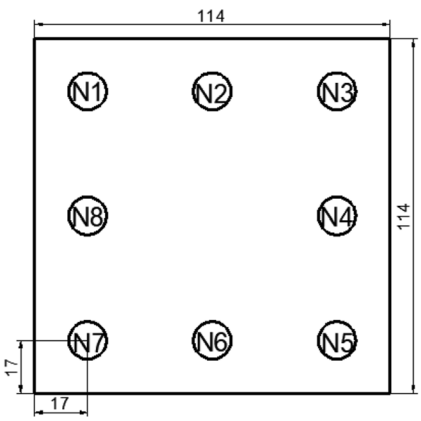

Figure 1 Schematic of the eight bolt configuration in the PEMFC (Unit: mm)

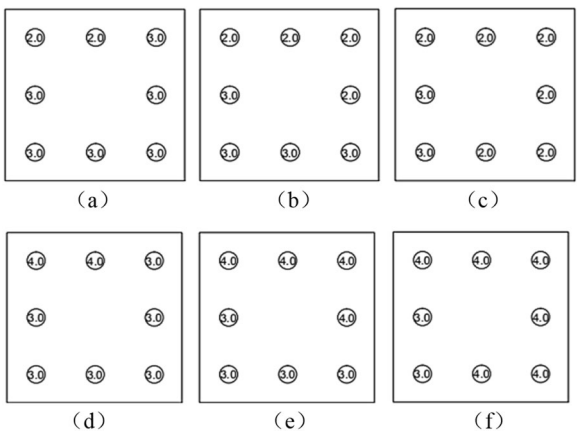

Figure 3 Non-uniform assembly bolt torque conditions: (**a**) The fourth condition, (**b**) The fifth condition, (**c**) The sixth condition, (**d**) The seventh condition, (**e**) The eighth condition, (**f**) The ninth condition

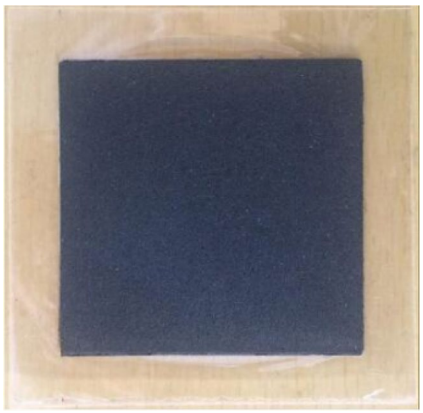

Figure 4 Picture of membrane electrode assembly (MEA)

Figure 5 Picture of PEMFC used for the test

Table 1 Size of the PEMFC components mm

Components	Quantity	Length	Width	Height	Diameter
End plate	2	114	114	19.5	-
Current collector	2	100	100	1.5	-
Bipolar plate	2	100	100	12.5	-
Gasket	2	100(55)	100(55)	0.25	-
GDL	2	50	50	0.2	-
Catalyst layer	2	50	50	0.025	-
PEM	1	50	50	0.05	-
Bolt	8	85	-	-	8

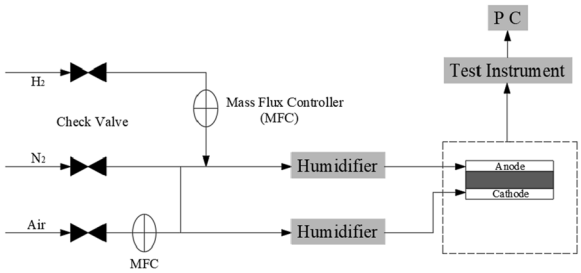

Figure 6 Test system for PEMFC experiments

3 Experiments

3.1 MEA Preparation

The MEA was made by hot pressing process, which consisted of proton exchange membrane, GDLs and catalyst layers. The effective area of the MEA was 25 cm^2. The GDL for the MEA used in this study was carbon paper (TGP-H-60, Toray) by coating a microporous layer (MPL). The proton exchange membrane (i.e., Nafion 212 membrane) was 50 μm in thickness. The catalyst layer was with 0.48 mg/cm^2 Pt/C (60%) loading on the anode and cathode sides. The catalyst was evenly coated on both sides of the proton exchange membrane. The catalyst layer was 25 μm in thickness. The MEA in this work is shown in Figure 4.

3.2 Single PEMFC Assembly

The single PEMFC used in this study includes two metallic end plates with the Nylon layers, two current collectors, two graphite BPPs, two elastomeric gaskets, a MEA and eight bolts. The geometric sizes of the PEMFC components are listed in Table 1. The prepared MEA stayed in the central position between a cathode and an anode BPPs. The anode BPP were with the three serpentine flow field channel with 1.2 mm in width, 0.6 mm in depth. The cathode BPP were with the three serpentine flow field channel with 1.2 mm in width, 1.2 mm depth. Width of the rigs was 1.2 mm for both anode and cathode flow field channels. The components of the fuel cell were assembled by eight pairs of bolts and nuts which were homogeneously distributed on the end plate. The PEMFC used in this study is shown in Figure 5.

3.3 Fuel Cell Testing System

In order to analyze the electrochemical performance of the PEMFC under different assembly forces, the experimental setup was designed to perform experiments on the different assembly force conditions described above. The experimental setup is based on the FC-2000 test platform from Arbin Company in USA.

The schematic of the Arbin fuel cell test system is shown in Figure 6. This system mainly composed of a gas flux control system, a gas moisture system, a temperature control system and a data monitoring and recording system. The H_2 and air needed to be humidified before they were introduced to the anode and cathode of the PEMFC, respectively. The upstream pressure meters were used to measure the intake gas pressures, and mass

flux controller (MFC) were used to precisely control the flow rates of compressed air and H_2. With the purpose of control the PEMFC temperature during the experiment, two thermocouples were put into the anode and cathode BPPs.

After the set background values have been reached, the gases (air and H_2) entered the PEMFC via the dew point humidification technique, and an electrochemical reaction is generated. During the experiments, the PEMFC was operated at a controlled temperature of 80 ℃, the flux of H_2 was 284 mL/min and the flux of air was 905 mL/min. The gas back pressures and relative humidity (RH) of the PEMFC at anode and cathode sides maintained at near 0 MPa and 100%, respectively.

4 Results and Discussion

4.1 Effect of the Uniform Assembly Bolt Torque on the Electrochemical Performance of the PEMFC

Figure 7 presents the test results of polarization curves (i.e., voltage-current density curve) and power density curves (i.e., power density-current density curve) of the PEMFC in three uniform assembly bolt toque conditions. Figure 6(a) shows the test results of polarization and power density curves in the first uniform assembly bolt toque condition. Figure 7(b) and (c) shows the test results of polarization and power density curves in the second and third uniform assembly bolt toque conditions, respectively. From Figure 7, the electrochemical performance of the PEMFC in three uniform assembly bolt toque conditions had no obvious change as the current density was lower than 300 mA·cm^{-2}. While the current density was higher than 300 mA·cm^{-2}, the magnitude of the assembly force had a significant impact on the PEMFC electrochemical performance. In Figure 7(a), the maximal power density in the first condition was 428.18 mW·cm^{-2}. In Figure 7(b), the maximal power density in the second condition was 448.03 mW·cm^{-2}. From Figure 7(c), the maximal power density in the third condition was 436.82 mW·cm^{-2}. The maximal power density in the second condition increased by 4.6% compared with that in the first condition and by 2.6% compared with that in the third condition. The PEMFC electrochemical performance in the second condition was the best among the three conditions.

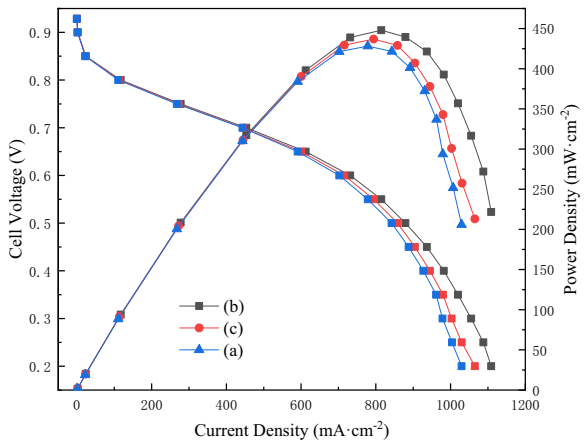

Figure 7 Polarization and power density curves of PEMFC under uniform assembly forces

The actual output voltage of the fuel cell can be expressed as [30]:

$$V = E_{\text{the}} - \eta_{\text{act}} - \eta_{\text{ohm}} - \eta_{\text{con}}. \quad (1)$$

In Eq. (1), V denotes the actual voltage of the PEMFC, and E_{the} denotes the ideal voltage of the PEMFC, η_{act} represents the internal activation loss of the PEMFC, η_{ohm} represents the internal ohmic loss, and η_{con} represents the concentration loss due to insufficient mass transfer concentration. It can be seen in Figure 7 that when the current density was lower than 300 mA·cm^{-2}, the decrease of the cell electrochemical performance (i.e., the decrease of Voltage) was mainly due to the η_{act}. When the current density exceeded 300 mA·cm^{-2}, the decrease of the cell electrochemical performance (i.e., the decrease of Voltage) was mainly due to the η_{ohm}. When the current density was on further increasing (e.g., larger than 1000 mA·cm^{-2}), the decrease of the cell electrochemical performance was mainly due to the η_{con}. From Figure 7, the PEMFC electrochemical performance did not obviously changed in the three assembly conditions as the current density was lower than 300 mA·cm^{-2}. However, the PEMFC electrochemical performance changed obviously after the current density exceeded 300 mA·cm^{-2}. The change of the PEMFC electrochemical performance was mainly due to the contact resistance between the GDL and BPP and transport resistance for the hydrogen and oxygen towards the catalyst layers.

Overall, it could be concluded that the different uniform assembly forces affected significantly the contact resistance (e.g., the contact resistance between the GDL and BPP) and transport resistance for the hydrogen and oxygen towards the catalyst layers, consequently, affected the electrochemical performance of the PEMFC. It existed the optimum assembly bolt torque in terms of the maximal power density. The optimum assembly bolt torque was found to be 3.0 N·m in this work.

4.2 Effect of the Non-Uniform Assembly Bolt Torque on the Electrochemical Performance of the PEMFC

Figures 8 and 9 show the test results of polarization and power density curves for the PEMFC in the non-uniform assembly bolt toque conditions. For comparison, the experimental results of the polarization curves for

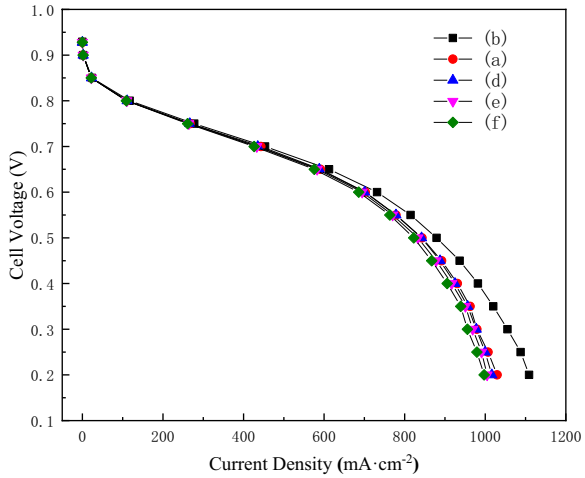

Figure 8 Test results of polarization curves for the fuel cell in the non-uniform assembly bolt toque conditions: (a) The first condition, (b) The second condition, (d) The fourth condition, (e) The fifth condition and (f) The sixth condition

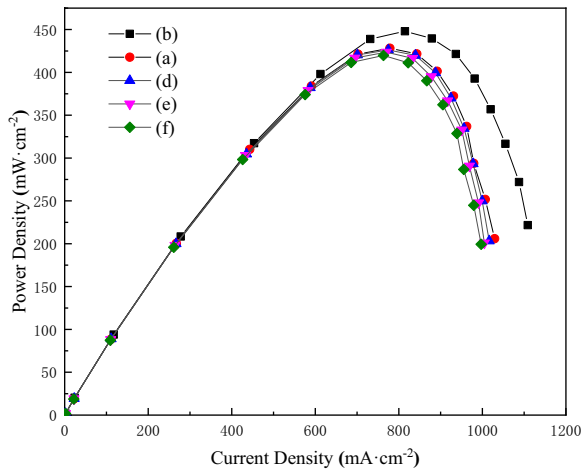

Figure 9 Test results of power density curves for the fuel cell in the non-uniform assembly bolt toque conditions: (a) The first condition, (b) The second condition, (d) The fourth condition, (e) The fifth condition, (f) The sixth condition

the fuel cell in the first assembly force condition and the second assembly force condition were plotted in Figure 8, and the experimental results of the power density curves for the fuel cell in the first assembly force condition and the second assembly force condition were also plotted in Figure 9. The experimental results of the polarization curves for the fuel cell in the fourth, fifth and sixth assembly force conditions are presented in Figure 8(d), (e) and (f), respectively. Similarly, the experimental results of the power density curves for the fuel cell in the fourth, fifth and sixth assembly force conditions are also presented in Figure 9(d), (e) and (f), respectively.

It can be seen from Figure 8 that the PEMFC electrochemical performance in three non-uniform assembly bolt toque conditions had no obvious change as the current density was lower than 300 mA·cm^{-2}. However, when the current density exceeded 300 mA·cm^{-2}, the non-uniform assembly bolt toque had a significant effect on the PEMFC electrochemical performance. When the current density was the same, the voltage of the fuel cell in the fourth assembly condition was larger than that of the fuel cell in the fifth condition as well as in the sixth condition. There was the best electrochemical performance of the PEMFC in the fourth assembly condition among the three non-uniform assembly conditions. It implies that there was better electrochemical performance as the assembly torque of each bolt was closer to the torque of 3.0 N·m in this work. In addition, the PEMFC electrochemical performance in uniform assembly bolt torque conditions was better than that of the fuel cell in non-uniform assembly bolt torque conditions.

From Figure 9, the maximum power density in the fourth assembly torque condition was 426.18 mW·cm^{-2}, and the peak power density in the fifth and sixth assembly torque conditions was 423.49 and 419.73 mW·cm^{-2}, respectively. There was the greatest peak power density of the PEMFC in the fourth assembly condition among the three non-uniform assembly conditions. The results show that there was better electrochemical performance as the assembly torque of each bolt was close to the torque of 3.0 N·m in this work. The reason could be that as the assembly bolt torque gradually increased, the contact pressure inside the PEMFC also increased. Then the interfacial contact resistance between the BP and the MEA was optimized, resulting in the decrease of the ohmic losses of the PEMFC.

Figures 10 and 11 show the experimental results of polarization and power density curves for the PEMFC in the non-uniform assembly bolt toque conditions. For comparison, the experimental results of the polarization curves for the fuel cell in the second assembly force condition and in the third assembly force condition were plotted in Figure 10, as shown in Figure 9(b) and (c). The experimental results of the power density curves for the fuel cell in the second assembly force condition and in the third assembly force condition were also plotted in Figure 11, as shown in Figure 10(b) and (c). The experimental results of the polarization curves for the fuel cell in the seventh, eighth and ninth assembly force conditions are presented in Figure 10(g), (h) and (i), respectively. Similarly, the experimental results of the power density curves for the fuel cell in the seventh, eighth and ninth

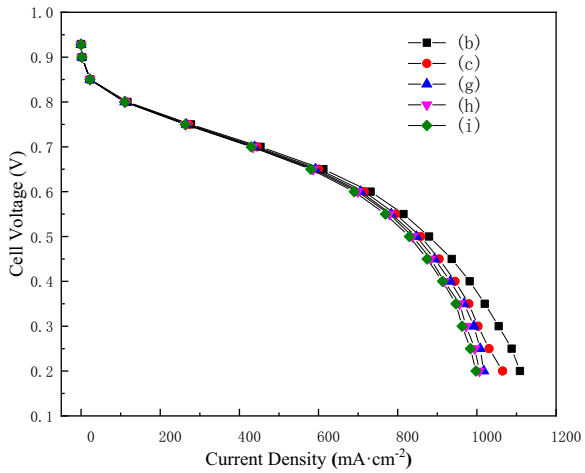

Figure 10 Test results of polarization curves for the fuel cell in the non-uniform assembly bolt toque conditions: (b) The second condition, (c) The third condition, (g) The seventh condition, (h) The eighth condition, (i) The ninth condition

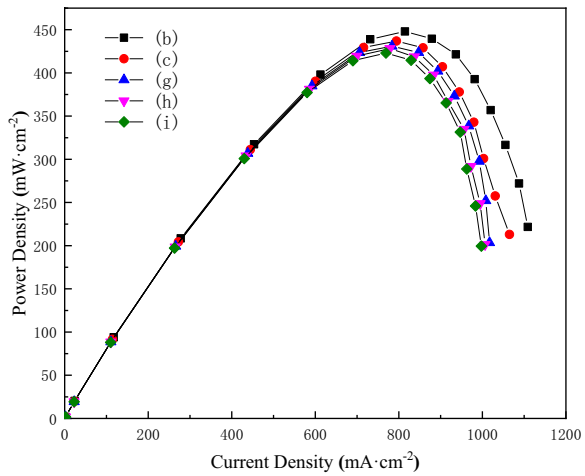

Figure 11 Test results of power density curves for the fuel cell in the non-uniform assembly bolt toque conditions: (b) The second condition, (c) The third condition, (g) The seventh condition, (h) The eighth condition, (i) The ninth condition

assembly force conditions are presented in Figure 11(g), (h) and (i), respectively.

It can be seen from Figure 10 that the PEMFC electrochemical performance in three non-uniform assembly bolt toque conditions had no obvious change as the current density was lower than 300 mA·cm^{-2}. However, when the current density exceeded 300 mA·cm^{-2}, the non-uniform assembly bolt toque had a significant effect on the PEMFC electrochemical performance. As the current density was the identical, the voltage of the fuel cell in the seventh assembly condition was larger than that of the fuel cell in the eighth condition as well as in the ninth condition. There was the best PEMFC electrochemical performance in the seventh assembly condition among the three non-uniform assembly conditions. It implies that there was better electrochemical performance as the assembly torque of each bolt was closer to the torque of 3.0 N·m in this work. In addition, it is noted that the electrochemical performance of the PEMFC in uniform assembly bolt torque conditions was better than that of the cell in non-uniform assembly bolt torque conditions. The results are in consistent with the results in Figure 8.

From Figure 11, the maximum power density in the seventh assembly torque condition was 430.96 mW·cm^{-2}, and the maximum power density in the eighth and the ninth assembly torque conditions was 426.12 and 423.04 mW·cm^{-2}, respectively. Thus, there was the greatest maximum power density of the PEMFC in the seventh assembly force condition among the three non-uniform assembly force conditions. The results show that there was better electrochemical performance as the assembly torque of each bolt was closer to the torque of 3.0 N·m in this work. The results are consistent with the results in Figure 9. In addition, it can be seen that the PEMFC maximum power density in the ninth assembly force condition was less than that of the PEMFC in the seventh assembly force condition. This could be due to that the excessive increasing assembly force reduced the internal porosity and mass transfer efficiency of the GDL, resulting in a reduction in the PEMFC electrochemical performance.

In order to further investigate the effects of different assembly forces on the electrochemical performance of the PEMFC, the experimental results of the polarization and power density curves for the fuel cell in

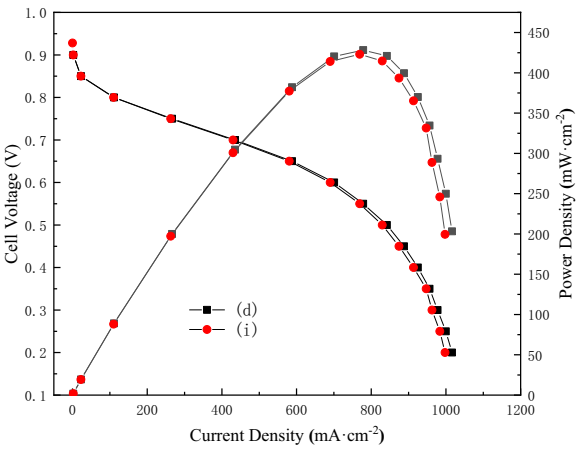

Figure 12 Polarization and power density curves of fuel cell in the non-uniform assembly toque conditions: (d) The fourth condition, (i) The ninth condition

the fourth assembly force condition are shown in Figure 12(d), and the experimental results of the polarization and power density curves for the fuel cell in the ninth assembly force condition are also shown in Figure 12(i) for comparison. It can be seen from Figure 12 that the electrochemical performance of the PEMFC for the fourth assembly force condition was better than that for the ninth assembly force condition. This is due to that the assembly torque of per bolt for the PEMFC in the fourth assembly force condition was closer to the torque of 3.0 N·m. Figure 13 presents the experimental results of the polarization and power density curves for the PEMFC in the sixth assembly force and the seventh assembly force conditions, respectively. From Figure 13, it can be clearly seen that the electrochemical performance of the PEMFC for the seventh assembly force condition was better than that for the sixth assembly force condition. The results are similar to those in Figure 12, i.e., the PEMFC had better electrochemical performance as the assembly torque of per bolt was more close to the torque of 3.0 N·m in this work. Figure 14 presents the experimental results of the polarization and power density curves for the PEMFC in the fifth assembly force and the eighth assembly force conditions, respectively. It is noted that the PEMFC in the two assembly force conditions was with the same number of bolts applied to 3.0 N·m per bolt. Thus, form Figure 14, the electrochemical performance was not changed obviously for the PEMFC in the two assembly force conditions, implying that the fuel cell had better electrochemical performance as the assembly torque of per bolt was closer to the torque of 3.0 N·m in this work.

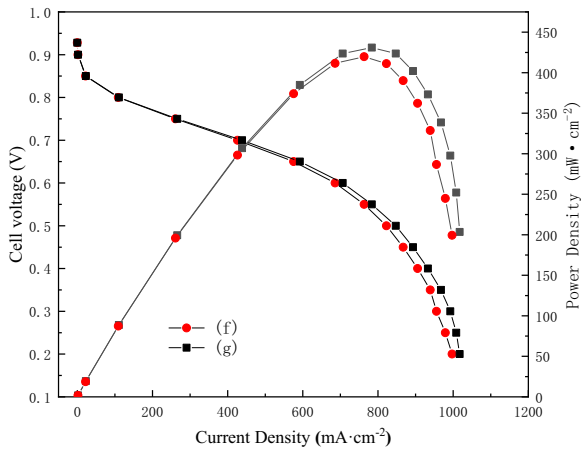

Figure 13 Polarization and power density curves of fuel cell in the non-uniform assembly toque conditions: (f) The sixth condition, (i) The seventh condition

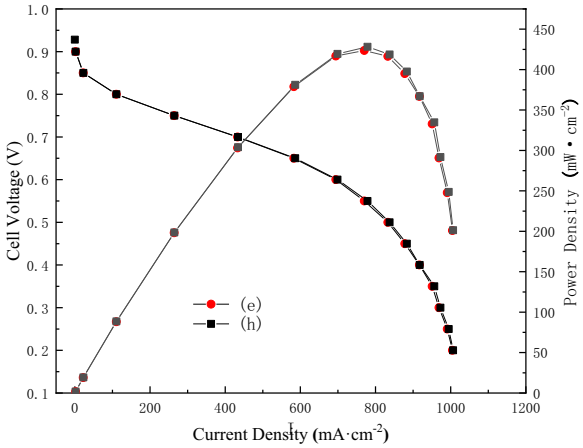

Figure 14 Polarization and power density curve of fuel cell in the non-uniform assembly bolt toque conditions: (e) The fifth condition, (h) The eighth condition

5 Conclusions

In this work, a single PEMFC with the three serpentine flow field was used and studied. The different assembly forces were applied to the PEMFC in three uniform assembly bolt torque and six non-uniform assembly bolt torque conditions, respectively. And then, electrochemical performance tests were carried out to investigate the effect of the different assembly forces on the electrochemical performance. The following conclusions can be made.

(1) The experimental results show that the magnitude of uniform assembly bolt torque significantly affected the PEMFC electrochemical performance. In the uniform assembly bolt torque conditions, the maximal power density initially increased as the assembly bolt torque increased, and then decreased on further increasing the assembly torque. It existed the optimum assembly bolt torque in terms of the maximal power density, which was 3.0 N·m in this work.

(2) The test results show that the non-uniform assembly bolt torque remarkably affected the electrochemical performance of the PEMFC. In the non-uniform assembly clamping bolt torque conditions, the optimum electrochemical performance appeared in the condition where the assembly torque of each bolt was more closer to be 3.0 N·m in this work. The effect of different assembly forces on the electrochemical performance could be due to the change of the contact resistance between the GDL and bipolar plate and mass transport resistance for the hydrogen and oxygen towards the catalyst layers.

(3) The results show that PEMFC had better electrochemical performance under an appropriate assembly bolt force. This work could optimize the further experimental conditions and be useful for the practical PEMFC stack assembly.

Acknowledgements
Not applicable.

Authors' Contributions
TS was in charge of the whole experiment and wrote the manuscript; JR assisted with investigation and data analyses; YW, YL and WL assisted with the whole trial; JT supervised. All authors read and approved the final manuscript.

Funding
Supported by National Natural Science Foundation of China (Grant No. 52275152).

Availability of data
The data that support the findings of this study are availabe from the corresponding author on reasonable request.

Declarations

Competing Interests
The authors declare no competing financial interests.

Received: 14 March 2023 Revised: 6 March 2024 Accepted: 27 March 2024
Published online: 19 May 2024

References

[1] H O Pörtner, D C Roberts, H Adams, et al. *Climate change 2022: impacts, adaptation and vulnerability.* Intergovernmental Panel on Climate Change (IPCC), 2022.
[2] A M Dafalla, F Jiang. Stresses and their impacts on proton exchange membrane fuel cells: A review. *International Journal of Hydrogen Energy*, 2018, 43(4): 2327-2348.
[3] J Zhang, Y Hu, C Han, et al. Stress response and contact behavior of PEMFC during the assembly and working condition. *International Journal of Hydrogen Energy*, 2021, 46(59): 30467-30478.
[4] Y Wang, K S Chen, J Mishler, et al. A review of polymer electrolyte membrane fuel cells: Technology, applications, and needs on fundamental research. *Applied Energy*, 2011, 88(4): 981-1007.
[5] H Huang, Z G Yang, Y M Wang, et al. Durability study of membrane electrode assembly under open circuit voltage operation. *Journal of East China University of Science and Technoloy. Natural Sciences Edition*, 2018 (5): 638-643. (in Chinese)
[6] R L Borup, A Z Weber. *FC-PAD: Fuel cell performance and durability consortium.* Los Alamos, NM, United States: Los Alamos National Lab (LANL), 2018.
[7] Z Y Su, C T Liu, H P Chang, et al. A numerical investigation of the effects of compression force on PEM fuel cell performance. *Journal of Power Sources*, 2008, 183(1): 182-192.
[8] W Yoon, X Huang. A multiphysics model of PEM fuel cell incorporating the cell compression effects. *Journal of the Electrochemical Society*, 2010, 157(5): B680.
[9] I Gatto, F Urbani, G Giacoppo, et al. Influence of the bolt torque on PEFC performance with different gasket materials. *International Journal of Hydrogen Energy*, 2011, 36(20): 13043-13050.
[10] X Yan, Lin C, Zheng Z, et al. Effect of clamping pressure on liquid-cooled PEMFC stack performance considering inhomogeneous gas diffusion layer compression. *Applied Energy*, 2020, 258: 114073.
[11] Z Zhou, D Qiu, S Zhai, et al. Investigation of the assembly for high-power proton exchange membrane fuel cell stacks through an efficient equivalent model. *Applied Energy*, 2020, 277: 115532.
[12] Y Zhou, Q Lin, H Shao, et al. Stress-based optimization of assembly surface mechanical properties oriented to stress-uniform assembly. *Precision Engineering*, 2023, 82: 350-359.
[13] Z Chen, Y Xing, J Cao, et al. Leakage analysis of PEMFC sealing system considering temperature cycling. *Energies*, 2023, 16(14): 5475.
[14] Bo Liu. *Structural optimization design and dynamics property of proton exchange membrane fuel cells.* Dalian: Dalian University of Technology, 2019. (in Chinese)
[15] G Ren, Y Xing, J Cao, et al. Study of contact pressure distribution in bolted encapsulated proton exchange membrane fuel cell membrane electrode assembly. *Energies*, 2023, 16(18): 6487.
[16] A H Mahmoudi, A Ramiar, Q Esmaili. Effect of inhomogeneous compression of gas diffusion layer on the performance of PEMFC with interdigitated flow field. *Energy Conversion and Management*, 2016, 110: 78-89.
[17] L Zhang, Y Liu, H Song, et al. Estimation of contact resistance in proton exchange membrane fuel cells. *Journal of Power Sources*, 2006, 162(2): 1165-1171.
[18] C H Chien, Y L Hu, T H Su, et al. Effects of bolt pre-loading variations on performance of GDL in a bolted PEMFC by 3-D FEM analysis. *Energy*, 2016, 113: 1174-1187.
[19] T Zhang, J Li, Q Li, et al. Combination effects of flow field structure and assembly force on performance of high temperature proton exchange membrane fuel cells. *International Journal of Energy Research*, 2021, 45(5): 7903-7917.
[20] Y Zhou, K Jiao, Q Du, et al. Gas diffusion layer deformation and its effect on the transport characteristics and performance of proton exchange membrane fuel cell. *International Journal of Hydrogen Energy*, 2013, 38(29): 12891-12903.
[21] D Cha, J H Ahn, H S Kim, et al. Effects of clamping force on the water transport and performance of a PEM (proton electrolyte membrane) fuel cell with relative humidity and current density. *Energy*, 2015, 93: 1338-1344.
[22] R K Mallick, S B Thombre, R V Motghare, et al. Analysis of the clamping effects on the passive direct methanol fuel cell performance using electrochemical impedance spectroscopy. *Electrochimica Acta*, 2016, 215: 150-161.
[23] Z Zhang, Z Chen, K Li, et al. A multi-field coupled PEMFC model with force-temperature-humidity and experimental validation for high electrochemical performance design. *Sustainability*, 2023, 15(16): 12436.
[24] S A Atyabi, E Afshari, S Wongwises, et al. Effects of assembly pressure on PEM fuel cell performance by taking into accounts electrical and thermal contact resistances. *Energy*, 2019, 179: 490-501.
[25] N Kulkarni, J I S Cho, R Jervis, et al. The effect of non-uniform compression on the performance of polymer electrolyte fuel cells. *Journal of Power Sources*, 2022, 521: 230973.
[26] X Chen, C Yang, Y Sun, et al. Water management and structure optimization study of nickel metal foam as flow distributors in proton exchange membrane fuel cell. *Applied Energy*, 2022, 309: 118448.
[27] L Shi, S Xu, J Liu. Influences of assembly pressure and flow channel size on performances of proton exchange membrane fuel cells based on a multi-model. *International Journal of Hydrogen Energy*, 2022, 47(12): 7902-7914.
[28] Z Zhang, J Zhang, L Shi, et al. A study of contact pressure with thermo-mechanical coupled action for a full-dimensional PEMFC stack. *Sustainability*, 2022, 14(14): 8593.
[29] Z Zhang, W Q Tao. Effect of assembly pressure on the performance of proton exchange membrane fuel cell. *Energy Storage and Saving*, 2023, 2(1): 359-369.
[30] R O'hayre, S W Cha, W Colella, et al. *Fuel cell fundamentals*. United States: John Wiley & Sons, 2016.

Tongze Su born in 1996, is currently a master candidate at *School of Mechanical and Power Engineering, Nanjing Tech University, China*.

Jiaran Liu born in 1997, received his master degree in chemical process machiney from *Nanjing Tech University, China,* in 2021.

Yanqiang Wei born in 1994, is currently a PhD candidate *at School of Mechanical and Power Engineering, Nanjing Tech University, China*. He received his master degree in power engineering from *Nanjing Tech University, China*, in 2021.

Yihuizi Li born in 1998, is currently a PhD candidate at *School of Mechanical and Power Engineering, Nanjing Tech University, China*.

Weichao Luo born in 1998, is currently a master candidate at *School of Mechanical and Power Engineering, Nanjing Tech University, China*.

Jinzhu Tan born in 1964, is a professor at *Nanjing Tech University, China*. He received his PhD degree in 2000 from *Nanjing Tech University, China*. His research interests include the PEM fuel cell technology and its applications, advanced energy materials, degradation and degradation mechanisms of structural materials.